PVP-Vol. 484, Recent Advances in Nondestructive Evaluation
Techniques for Material Science and Industries
July 25-29, 2004, San Diego, California USA
PVP2004-2830

EVALUATION OF FATIGUE DAMAGE IN COARSE-GRAINED ALUMINUM WITH SCANNING X-RAY ENERGY DISPERSIVE DIFFRACTION MICROSCOPE

Yoshinori HOSOKAWA, Hirotaka TANABE, Yoshio MIYOSHI, Tohru TAKAMATSU
The University of Shiga Prefecture
Hikone, Shiga, Japan.

Kenichi OBORIi
Horiba, Ltd
Kisshoin, Kyoto, Japan.

ABSTRACT

Based on the Berg-Barrett method, Scanning Energy Dispersive X-ray Diffraction Microscopy (SEDXDM) has been developed for nondestructively evaluating both the surface and subsurface of poly-crystallized materials. The SEDXDM includes an X-ray source generating continuous X-ray spectrum as a key component to form a highly resolved 2-D horizontal cross-sectional digital image. This article presents the evaluation of the fatigue damage (*e.g.*, slip line and slip band caused by fatigue deformation) of the coarse-grained aluminum, which is made by means of annealing and has been repeatedly bent to generate the stress and make the slope of the stress created in the thickness direction of the plate specimen, under fully reversed anti-plane bending condition with the SEDXDM.

INTRODUCTION

Based on the Berg-Barrett method, Scanning Energy Dispersive X-ray Diffraction Microscope (hereinafter called simply "SEDXDM") has been developed. The SEDXDM includes an X-ray source generating continuous X-ray spectrum as a key component to form a highly resolved two-dimensional (hereinafter called simply "2-D) horizontal cross-sectional digital image.

In the previous study, a deformation, which was been caused by tensile loading, of an interior portion of poly-crystallized aluminum plate specimen was nondestructively visualized on a 2-D horizontal cross-sectional image with the SEDXDM [1]. The image showed the minute texture change (*e.g.*, rotation), which was caused by the deformation, of each crystal grain. Further, when using the SEDXDM, a plurality of diffraction images could be simultaneously obtained, wherein each diffraction image was in accordance with each wavelength of X-ray spectra. Furthermore, the diffraction images showed the conditions of the crystal grains internally located in the specimen. However, in the previous study, the size of the grains of the specimen was too small to provide the precise information of the specimen interior, considering the deformation caused by the tensile loading.

In the present study, a coarse-grained aluminum plate specimen has been prepared. The specimen has been repeatedly bent to generate the stress and to make the slope of the stress created in the thickness direction of the specimen. Therefore, the fatigue damage in accordance with the stress distribution in the thickness direction of the specimen is given. Then, the two dimensional diffraction images showing the damages of specimen are obtained by the SEDXDM. The analyses of the images allow one to determine whether the damage is caused due to the stress distribution or not.

ENERGY DISPERSIVE X-RAY DIFFRACTION METHOD

When X-ray is incident to a crystal, the diffraction X-ray is expressed as Bragg's diffraction condition equation.

$$2d \cdot \sin\theta = \lambda \tag{1}$$

where d is the distance of the crystal lattice, θ is the incident angle of the X-ray, and λ is the wavelength of the X-ray.

The relation between the energy of the X-ray (denoted as "E_n") and the wavelength (denoted as "λ") is expressed as follows:

$$E_n = \frac{hc}{\lambda} = \frac{12.398}{\lambda} \tag{2}$$

where h is Planck's constant, and c is the velocity of light.

Equation (2) shows that E_n is in inverse proportion to λ. Therefore, the shorter λ is, the higher the accelerating voltage is. Putting Eq. (2) into Eq. (1), we obtain the equation as follows:

$$E_n = \frac{12.398}{2d\sin\theta} \tag{3}$$

In Eq. (3), d is the distance of the crystal lattice, and it is expressed as follows:

$$d = \frac{6.199}{E_n \sin\theta} \tag{4}$$

Equation (4) shows that d is in inverse proportion to the product of E_n by $sin\theta$.

Miller indices h, k, and l can be determined by the following equation.

$$d = \frac{a}{\sqrt{h^2+k^2+l^2}} \tag{5}$$

where a is a lattice constant of the aluminum specimen. In the present study, we set that a is 0.40497nm.

PRINCIPLE OF SEDXDM

Uniqueness of Hardware

Figure 1 is a schematic diagram of SEDXDM comprising a data acquisition portion including an X-ray generator having an X-ray optical system, an X-Y stage for locating a specimen, and an X-ray detector, and a data control and analysis portion including a personal computer.

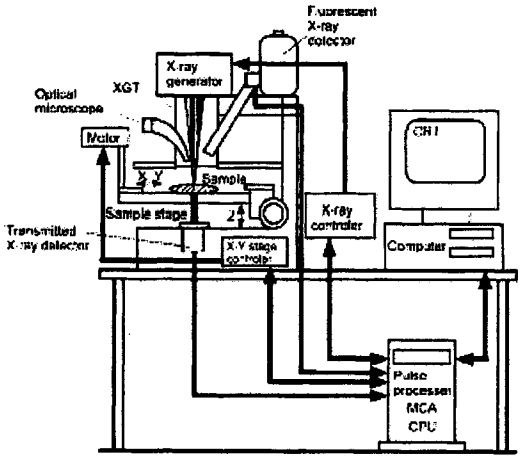

Fig.1 Schematic diagram of scanning energy dispersive X-ray diffraction microscope.

The novel features of the SEDXDM are (1) X-ray guide tube (hereinafter called simply "XGT") for creating a small X-ray bundle (minimum: 10μmΦ) without power deterioration and (2) X-Y stage for scanning a specimen to map various elements (*i.e.*, from $_{11}$Na to $_{92}$U) existing on the scanned area in a 2-D image. Further, when increasing time for X-ray emission of the SEDXDM, X-ray diffraction spectra of a specimen (*e.g.*, poly crystallized aluminum) can be observed, in addition to the observation of X-ray spectra of various elements of the specimen. Furthermore, although thickness of a specimen is limited, the SEDXDM can form X-ray transmission image of an interior portion of a specimen. Therefore, the SEDXDM can be used as a NDE apparatus to detect an internal flaw of a specimen or measure the thickness of a specimen.

Imaging Mechanism

Figure 2 shows a schematic diagram of imaging mechanism of the SEDXDM. Basic imaging method is similar to that of a conventional X-ray diffraction reflection microscope based on the Berg-Barrett method [1]. The main difference is that the SEDXDM comprises the XGT. The XGT, which is made of glass, collimates a continuous X-ray bundle (*e.g.*, 100μmΦ in the present study) output from the X-ray generator, closely guided to the surface of a specimen (*i.e.*, poly-crystallized material) with a certain angle (*e.g.*, 67.5° in the present study), and emits the micro-focus X-ray beam onto the surface of the specimen located on the X-Y stage. When the X-ray beam is emitted onto the specimen, the X-ray is diffracted satisfying with Eq. (3). The X-ray detector can detect both energy and intensity of the diffracted X-ray. When X-Y stage is two-dimensionally scanned, the information of scanned area of the specimen that may include a whole crystal grains can be shown in a digital image, wherein the information relates to the X-ray diffraction. Further, continuous X-ray is adopted into the SEDXDM. Therefore, the SEDXDM can visualize a crystal grains located in relatively deep portion of the specimen when changing the wavelength of the X-ray, which is incident into the specimen. Note that the wavelength of the X-ray depends on the accelerating voltage of the X-ray tube.

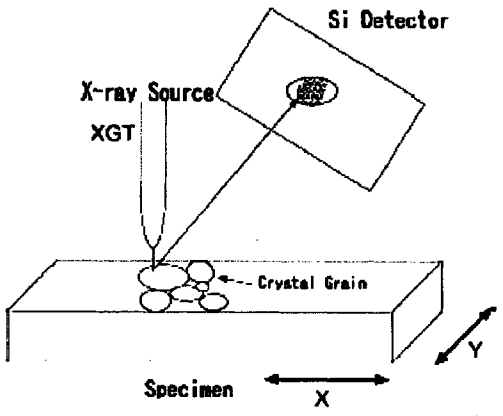

Fig.2 Schematic diagram of imaging mechanism.

EXPERIMENT DETAILS

Specimen

We made a plate specimen (see Fig. 3) shaping it from a pure aluminum plate (thickness: 5mm) that is commercially available. The chemical composition of the specimen is described in Table 1. The specimen (*i.e.,* smoothed test-piece) is prepared for bending fatigue test. We annealed the specimen for two hours at 650°C to enlarge aluminum crystals. Finally, we were able to have a few large crystals. Within a large crystal grain, we could observe small grains ranging from a few microns to a few millimeters in their diameters. However, the anisotropy of those small crystals is large compared to that of the large crystal. Therefore, we consider that the small crystals are independent from the large crystal. The mechanical properties of the specimen are shown in Table 2.

Table1 Chemical composition of specimen (wt%)

Si	Cr	Fe	Ni	Cu	Al
0.89	0.06	0.22	0.01	0.03	Bal.

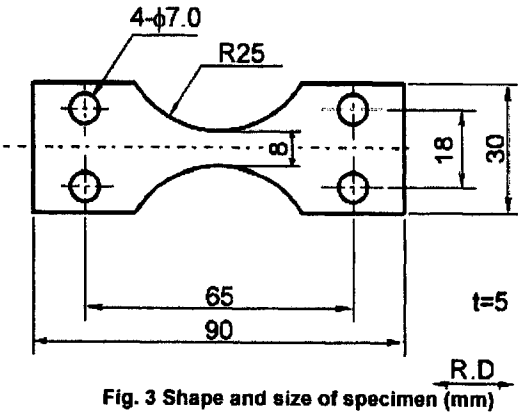

Fig. 3 Shape and size of specimen (mm)

Table 2 Mechanical properties of specimen.

0.2% flow stress	15MPa
Tensile strength	50MPa
Elongation	55%

Fatigue Test

We used a shank type of fatigue test apparatus having 30Nm for maximized bending moment (Tokyo Koki, Co., Ltd.; Model: PWOG-L). Fatigue test was anti-plane bending, its stress ratio (denoted as "R") was -1, and its repetition rate was 27 Hertz.

Figure 4 is the S-N curve of the fatigue life test completed before the fatigue damage evaluation, and shows that the specimen was not ruptured with the stress amplitude of 32MPa and the number of cycles at 10^7. Therefore, we chose two types of loading stress amplitudes such as 35MPa and 40MPa in the present study. We also monitored the surface of the specimen during the fatigue test because the specimen included large crystal grains so that cracks could be generated by local deformations.

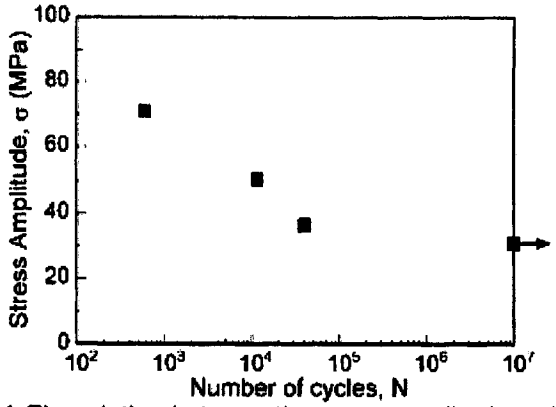

Fig. 4. The relation between the stress amplitude and the number of cycles.

Conditions for Microscopic Observation

The fatigue test was appropriately paused to observe fatigue damage. First, the damage was observed with a conventional optical microscope, and, second, with the SEDXDM. The observation conditions of SEDXDM are shown in Table 3.

Table 3 Conditions of observation.

X-ray cathode	Rh
Diameter of XGT	100[$\mu\phi$]
Tube voltage	50[kV]
Tube current	1.0[mA]
Scan time	8(3600[sec]/1 frame)

We can select a scanning area out of two (one is 10.204mm×10.204mm; another is 14.336mm×14.336mm). It takes 3,600 seconds for the X-ray beam to scan the area to obtain one SEDXDM image.

RESULTS

Analysis of Diffraction X-ray Spectrum

Figure 5 is a series of X-ray spectra of the specimen, wherein the spectra are obtained by the SEDXDM. In Fig. 5, the spectra having names of chemical elements are fluorescent X-rays from the chemical elements included in the specimen and the anticathode (denoted as "Rh"), and the spectra having numbers are diffraction X-rays. Some chemical elements contained in the specimen (*e.g.*, chrome, manganese and the like) are not shown in Fig. 5 because their energies are the same as energies of the diffraction X-rays. When changing the incident angle of the X-ray, the energy of the diffraction X-ray changes. Therefore, we can separate the fluorescent and diffraction X-ray spectra.

Figure 5 shows that energy of diffraction X-ray depends on the Miller index. The higher the number of the index is, the larger energy of the diffraction X-ray is.

Now, let t be the depth of the specimen, wherein the intensity of the X-ray diffracted from t indicates 63% of the intensity of

the entire X-ray detected by the apparatus. Let I_t be the incident intensity of the X-ray diffracted from the crystal located from the surface to the internal plane at t of the specimen. Let I_∞ be the incident intensity of the X-ray diffracted from the crystal located on the internal plane having depth of infinity. Then, the ratio between I_t and I_∞ is expressed as follows:

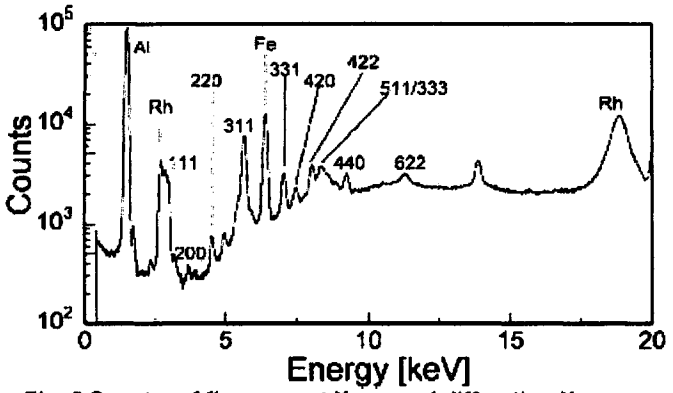

Fig. 5 Spectra of fluorescent X-ray and diffraction X-ray.

$$\frac{I_t}{I_\infty} = 1 - \exp\left(-\rho\mu \frac{2t}{\sin\theta\cos\psi}\right) \tag{6}$$

where ρ is the density, μ is a constant known as the "linear absorption coefficient" with dimension cm^{-1}, and its value depends on the material and the X-ray wavelength, θ is the incident angle of the X-ray, and ψ is the angle between the normal lines of the specimen surface and the diffraction plane.

Then, the effective incident depth (denoted as "t_e") of the X-ray relating to t is expressed as follows [2]:

$$t_e = \frac{\sin\theta\cos\psi}{2\rho\mu E_n} \tag{7}$$

Equation (7) shows that the larger the energy of X-ray is, the deeper the information of the specimen may be obtained.

For example, in the present study, the density ρ of the specimen is $2.70 g/cm^3$, the incident angle θ of the X-ray is 67.5°, and the angle of normal lines ψ is 0. Therefore, the effective incident depth t_e at the 622 plane in Fig. 5 can be calculated as 87μm approximately.

Evaluation of Fatigue Damage with SEDXDM

Change of Substructure with Fatigue Deformation

Figures 6(a)~6(d) and Figures 7(a)~7(d) show the change of fatigue damage in accordance with the increase of the number of bending repetitions on the diffraction plan indicated at 311. Stress amplitudes used in the fatigue test are 35MPa and 40MPa respectively. The observation areas with SEDXDM are the center portions of the specimens. The scanned areas shown in Figs. 6 and 7 are 14.336mm×14.336mm and 10.240mm×10.240mm respectively.

Figure 6(a) shows the SEDXDM image before starting the fatigue test (*i.e.*, N=0). In Fig. 6(a), the black portion is the coarse-grained crystal (size: approximately 15mm×15mm) on the diffraction plane indicated at 331. White portions are other crystals having different crystallographic axes. With the increase of the number of bending repetitions (*i.e.*, $N=8.0\times10^3$), slip lines and bands start appearing (see white inclined lines shown in Fig. 6(b)). The slip lines or bands can be observed as white lines because some portions of the crystal were deformed in steps, so that the axes of the deformed portions were changed. Therefore, the diffraction plane does not satisfy Bragg's condition. Furthermore, with the increase of the number of bending repetitions, the number of slip lines and bands increases (see Fig. 6(c)) too, and slip lines and bands become wider and spread to the entire portion of the crystal (see Fig. 6(d)). However, no change can be seen in white potions in Fig. 6(d). It means that size of other crystals is smaller and they have different crystallographic axes, so that their resistivity for fatigue deformation is large.

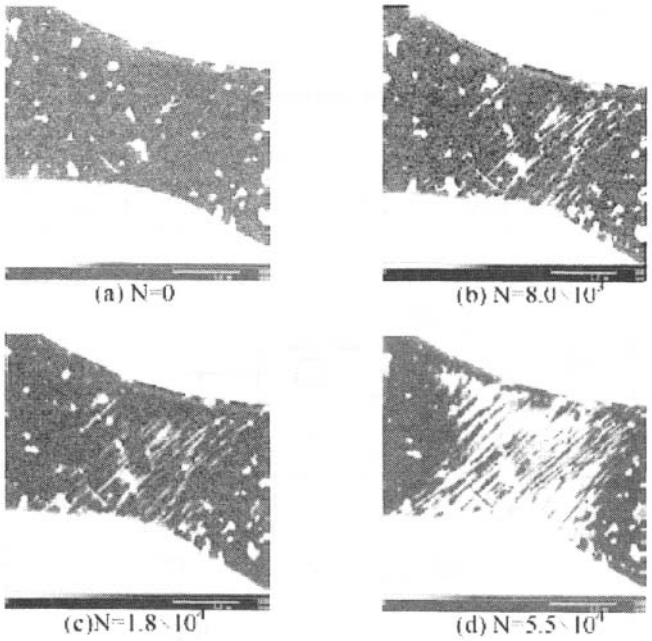

Fig.6 Change of substructure with fatigue deformation (311 plane, σ=35MPa).

Figure 7(a) shows the SEDXDM image before starting the fatigue test (*i.e.*, N=0). Two large crystals having different crystallographic axes are observed. When increasing the number of bending repetitions (*i.e.*, $N=8.0\times10^3$), slip bands start appearing (see white and black inclined lines shown in black and white portions in Fig. 7(b)). The number of slip bands observed in Fig. 7(b) is higher than that in Fig. 6(b) because the applied stress amplitude is different (*i.e.*, 40MPa). The directions of inclined lines are various because the slipping directions are different.

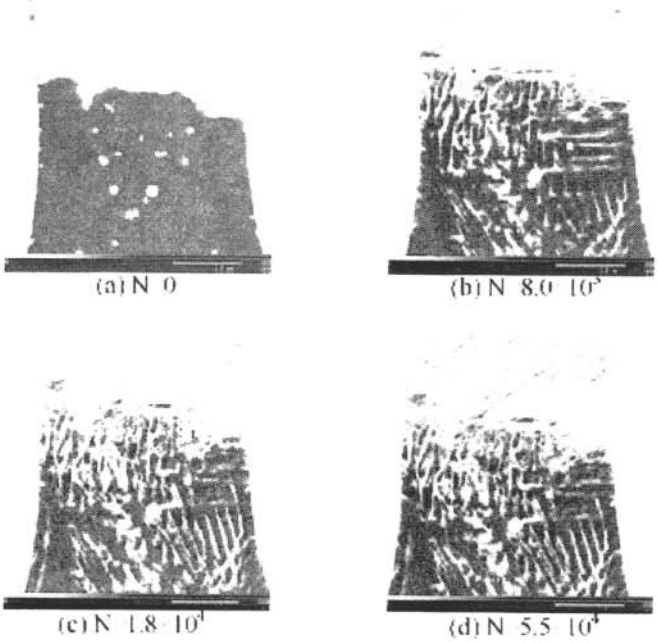

Fig.7 Change of substructure with fatigue deformation (311 plane, 40MPa).

Relation between Fatigue damage and Diffraction Plane

In Fig. 8(a)(*i.e.*, N=3.0×10^4), the slip lines and bans can be observed on the plane indicated at 622.

However, the contrast of the slip bands is not clear, compared to that on the plane indicated at 311. Contrast difference is explained as follows: The plane indicated at 622 is more internally located comparing to the plane indicated at 311, so that loading stress is different when bending fatigue tests are applied. Therefore, deformation rate is different.

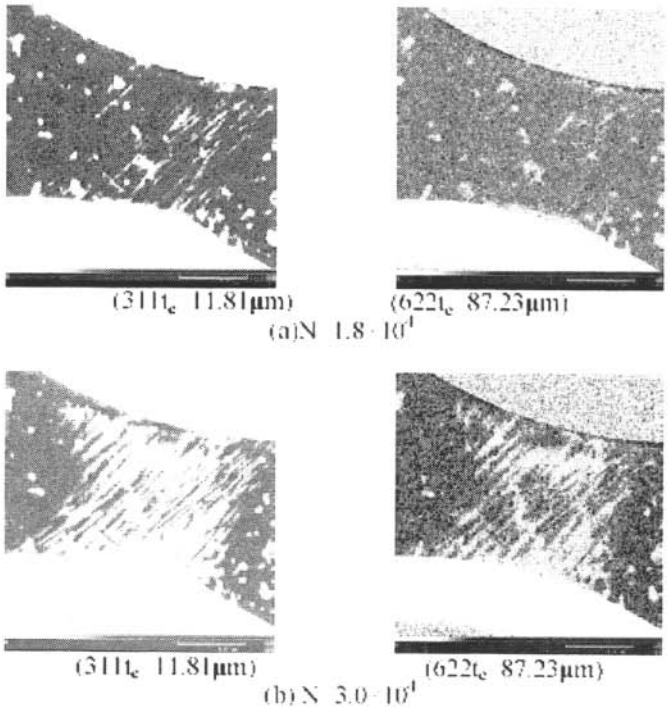

Fig.8 Relation between fatigue damage and diffraction plane(σ=35MPa).

CONCLUSIONS

Scanning Energy Dispersive X-ray Diffraction Microscopy (SEDXDM) has been developed and applied to nondestructively evaluate fatigue damage of coarse-grained aluminum. Then, we have obtained the following results.

(1) Slip line and slip band caused by fatigue deformation damage of the coarse-grained aluminum can be visualized by the SEDXDM.
(2) The SEDXDM can obtain damage information of both the surface and subsurface of poly-crystallized materials.
(3) The SEDXDM can specify the shape, size, and location of the crystal grains located within the specimen.

REFERENCES

[1] Miyoshi et al., JSMS, Proceeding of 36th Symposium of X-ray and Strength of Materials (2000), pp.169-173
[2] Nagao et al, JSMS, 26, (1977), p. 19